

# An automated algorithm to compute infrared divergent multi-loop integrals

T. Binoth<sup>a</sup> and G. Heinrich<sup>b</sup>

<sup>a</sup>Laboratoire d'Annecy-Le-Vieux de Physique Théorique<sup>1</sup> LAPTH,  
Chemin de Bellevue, B.P. 110, F-74941 Annecy-le-Vieux, France

<sup>b</sup>Laboratoire de Physique Théorique<sup>2</sup> LPT,  
Université de Paris XI, Bâtiment 210,  
F-91405 Orsay, France

## Abstract

We describe a constructive procedure to separate overlapping infrared divergences in multi-loop integrals. Working with a parametric representation in  $D = 4 - 2\epsilon$  dimensions, adequate subtractions lead to a Laurent series in  $\epsilon$ , where the coefficients of the pole and finite terms are sums of regular parameter integrals which can be evaluated numerically. We fully automated this algorithm by implementing it into algebraic manipulation programs and applied it to calculate numerically some nontrivial 2-loop 4-point and 3-loop 3-point Feynman diagrams. Finally, we discuss the applicability of our method to phenomenologically relevant multi-loop calculations such as the NNLO QCD corrections for  $e^+e^- \rightarrow 3$  jets.

---

<sup>1</sup>UMR 5108 du CNRS, associée à l'Université de Savoie.

<sup>2</sup>UMR 8627 du CNRS

# 1 Introduction

The increasing experimental precision at present and future colliders requires fast progress in the calculation of higher order corrections from the theoretical side. A crucial role is thereby played by the calculation of multi-loop integrals, which becomes an increasingly challenging task as the number of loops and the number of kinematic invariants gets larger.

In the case of two-point functions, up to four loop orders could be evaluated [1, 2] by exploiting the integration-by-parts method [3] and recurrence relations. This powerful technique also has been generalized to calculate three-loop propagator-type diagrams in heavy quark effective theory [4]. Similarly, the presence of only one kinematic invariant allowed for the calculation of two-loop three-point functions [5, 6, 7, 8, 9], which could be applied to compute the partonic cross sections for DIS and the Drell-Yan process to NNLO [10, 11]. Physical processes with a more difficult kinematic structure could not be computed to two-loop order yet, amplitudes exist only for very special cases [12]. A major reason is that two-loop integrals with four external legs, involving more than one kinematic variable, constitute a more complex problem. Only very recently, the analytic calculation of the massless planar [13] and non-planar [14] double box could be achieved by using Mellin-Barnes integration techniques. Furthermore, results for single-box integrals with self-energy and vertex insertions have been given in [15] and techniques based on differential equations to reduce two-loop four point functions to a set of master integrals have been derived in [16, 17]. The tensor reduction of massless double box integrals has been completed in [18], where the second master integral needed in the reduction of crossed two-loop boxes is given. However, it is not clear at the moment whether the techniques developed so far are sufficient to solve more complicated higher order problems as well.

Hence, to obtain results for integrals which are beyond the scope of analytic integration methods, but also as a simple check of involved analytic calculations, it is desirable to have a method at hand which allows the calculation of multi-loop integrals numerically. For two-loop box integrals with internal masses, thus with no infrared divergence, semi-numerical approaches have been designed in [19]. The massless case requires a different approach because of the presence of infrared divergences, which first have to be extracted from the integral in order to make it amenable to numerical evaluation.

In perturbative QCD, the calculation of infrared safe quantities has to be organized such that the infrared poles stemming from virtual and real higher order corrections cancel. At next-to-leading order usually semi-analytical methods are used to achieve this cancelation. As an alternative, a completely numerical method has been developed in [20]. The algorithm allows for the summation of the contributions from different cuts of a graph before integration, such that the cancelation of soft and collinear divergences is built in as imposed by unitarity. Nevertheless, since the method requires the deformation of the multi-dimensional integration contours to avoid fake singularities, its general applicability to NNLO calculations is highly nontrivial.

Hence a general local subtraction procedure to separate infrared divergences from individual graphs of arbitrary loop order would be very useful. The IR singularity structure of higher-loop Feynman diagrams was investigated in [21] in four dimensions, and later in [22] in the context of dimensional regularization and factorization in QCD. Working in dimensional regularization, subtraction procedures are well known for UV poles, and also for IR divergences present in Euclidean space (see e.g. [23]). On the other hand, no general subtraction scheme for soft and collinear IR singularities arising in Minkowski space is known for individual graphs. The method we present in this paper has been designed to isolate poles in the dimensional regulator for an arbitrary Feynman graph. Although the method also works for one-loop integrals, its virtues show up rather in two- or higher loop integrals with  $N \geq 3$  external legs, at least one of them being massless. It allows one to disentangle overlapping soft and collinear divergent regions in Feynman parameter space by dividing the latter into sectors where parameters can get singular only in an independent manner. Then, by adding and subtracting adequate counterterms, one can isolate the singular parts and perform

The algorithm can be divided into four blocks. In the first one, the  $\delta$ -distribution constraint on the Feynman parameters is eliminated in a particular way and in the second one, the singular contributions are isolated in parameter space. The third block consists of a subtraction procedure for the  $1/\epsilon^m$  poles, producing a set  $C_m$  of finite functions of the Feynman parameters as coefficients of each order  $m$  pole. In the fourth block, the integrations over the Feynman parameters in these functions are performed. The coefficient functions of the leading and subleading pole of a graph are in general simple enough to be integrated analytically with an algebraic manipulation program, whereas the remaining functions have to be integrated numerically.

## 2 The algorithm

$$G = \prod_{j=1}^N dK_1 \dots dK_L P_j(fk_g; fpg; m_j^2) \quad (1)$$
$$G = \binom{Z}{N} d^N x \prod_{l=1}^N x_l dK_1 \dots dK_L \prod_{j=1}^L k_j k_{M-j+1} \prod_{j=1}^L k_j Q + J^5 \quad (2)$$
$$G = (1)^N (N \quad LD=2) \quad d^N x \quad (1 \quad x_1) \frac{U^N \quad (L+1)D=2}{F^N \quad LD=2} \quad (3)$$
$$F(\mathbf{x}) = \det(\mathbf{M})^4 \prod_{j=1}^2 X_j^{Q_j} \prod_{j=1}^3 Q_{j1}^{M_{j1}} \quad (4)$$

$$U(\mathbf{x}) = \det(M) \quad (5)$$

As is well known, the parametric representation is determined by two functions which we call  $U$  and  $F$ . They are defined by the topology of the corresponding Feynman diagram [24, 25, 26].  $F$  contains the Mandelstam variables related to the different cuts of the graph.

A necessary condition for the presence of infrared divergences is that the Landau equations [27, 26] are fulfilled. A representation of the Landau equations following from Eq. (2) is given by

$$\begin{aligned} k_l &= \sum_{j=1}^{X_l} M_{lj}^{-1} Q_j \\ F &= 0 \end{aligned} \quad (6)$$

The function  $U$  cannot lead to infrared divergences of the graph, since giving a mass to all external legs would not change  $U$ . Apart from the fact that the graph may have an overall UV divergence contained in the overall  $\phi$ -function (see Eq. (3)), UV subdivergences may also be present. A necessary condition for these is the vanishing of  $U$ . In this way the UV poles can be identified and treated according to standard renormalization procedures. Infrared poles in  $\phi$  come from the parameter region where some Feynman parameters are small such that  $F$  vanishes. The Feynman parameter integrations which lead to poles can be related to a kinematical configuration in momentum space by using Eqs. (6). The IR poles come from soft and/or collinear momentum configurations where propagators do not describe virtual particles anymore but rather the propagation of an on-shell particle together with eventual splittings<sup>3</sup>. The soft/collinear poles of multi-loop graphs are the result of such kinematical situations in loop momentum space. These singular regions are generally not separated from each other in momentum (or equivalently in Feynman parameter space), they are overlapping.

Our aim is to disentangle these regions of overlapping IR divergences. To this end we use a method called sector decomposition<sup>4</sup>. Iterated application will lead to a set of integrals in which the infrared singular behaviour is not contained in complicated functions anymore, but in simple products of Feynman parameters raised to some power, times remnants of the functions  $F, U$ , whose structure is such that they neither lead to a pole anymore, nor change the exponent of the respective poles. In more detail, the procedure consists of four basic building blocks:

## Part I Generation of primary sectors

In the first part of the algorithm we split the integration domain into  $N$  parts and eliminate the  $\phi$ -distribution in such a way that the remaining integrations are from 0 to 1. To this end we decompose the integration range as follows

$$\int_0^{Z_1} d^N \mathbf{x} = \int_0^{Z_1} d^N \mathbf{x} \prod_{j=1}^{Y^N} \theta(x_j - 0) = \sum_{l=1}^{X^N} \int_0^{Z_1} d^N \mathbf{x} \prod_{\substack{j=1 \\ j \notin l}}^{Y^N} \theta(x_l - x_j - 0) \quad (7)$$

where the  $\theta$ -function is defined as

$$\theta(x - y) = \begin{cases} 1 & \text{if } x - y \text{ is true} \\ 0 & \text{otherwise} \end{cases}$$

The integral is now split into  $N$  domains corresponding to  $N$  integrals  $G_l$  from which we extract a common factor:  $G = (1)^N (N - 1) \sum_{l=1}^N G_l$ . In the integrals  $G_l$  we integrate out  $x_1$  by using

<sup>3</sup>This can be visualized by defining the reduced graph [28] of a diagram, which is the diagrammatic representation of solutions of the Landau equations.

<sup>4</sup>This method was of some importance in the history of UV regularization, i.e. to establish the BPHZ method. It was used by Hepp [29] to deal with overlapping UV divergences.

the  $\delta$ -distribution after having done the substitution

$$x_j = \begin{cases} x_1 t_j & ; j < l \\ x_1 & ; j = l \\ x_1 t_{j-l} & ; j > l \end{cases} \quad (8)$$

Because of homogeneity,  $x_1$  factorizes completely in the functions  $U(\mathbf{x}) = U_1(\mathbf{t}) x_1^L$  and  $F(\mathbf{x}) = F_1(\mathbf{t}) x_1^{L+1}$  and thus, using  $dx_1 = x_1 (1 - x_1 (1 + \sum_{k=1}^{N-l} t_k)) = 1$ , one obtains

$$G_l = \int_0^1 d^{N-l} t \frac{U_1^{N-(L+1)D=2}}{F_1^{N-LD=2}} ; l = 1; \dots; N \quad (9)$$

Note that the singular behaviour leading to  $\delta$ -poles still comes from the regions of small  $t$ 's. This feature would be lost if one integrated out the  $\delta$ -distribution in a naive way, since this would produce poles at upper limits of the parameter integrals as well. The generated sectors will be called primary sectors in the following. The functions  $U_1$  and  $F_1$  are polynomials in the parameters  $t_j$ .

## Part II Iterated sector decomposition

The second part of the algorithm consists of the iterated application of sector decomposition and a remapping of parameter space to the unit cube in order to disentangle the overlapping singular regions of the integrands. Starting with Eq. (9) one repeats the following steps until complete separation of overlapping regions is achieved.

II.1: Determine a minimal set of parameters, say  $S = \{t_{j_1}; \dots; t_{j_r}\}$ , such that  $U_1$ , respectively  $F_1$ , vanish if the parameters of  $S$  are set to zero.  $S$  is generally not unique. A additional selection criteria can be introduced to choose an  $S$  which does not lead to a large number of subsequent sector decompositions.

II.2: Decompose the corresponding  $r$ -cube into  $r$  subsectors.

$$\int_{j=1}^r dt_{j_1} \dots dt_{j_r} = \int_{k=1}^r \int_{j \notin k} dt_k \dots dt_{j_r} \quad (10)$$

II.3: Remap the variables to the unit cube in each new subsector by substituting

$$t_{j_1} = \begin{cases} t_k t_{j_1} & ; j_1 \notin k \\ t_k & ; j_1 = k \end{cases} \quad (11)$$

This gives a Jacobian factor of  $t_k^{r-1}$ . By construction  $t_k$  factorizes at least from one of the functions  $U_1, F_1$ . The resulting subsector integrals have the general form

$$G_{lk} = \int_0^1 d^{N-l} t \int_{j=1}^{N-l} dt_{j_1} \dots dt_{j_r} \frac{U_{lk}^{N-(L+1)D=2}}{F_{lk}^{N-LD=2}} ; k = 1; \dots; r \quad (12)$$

For each subsector the above steps have to be repeated as long as a set  $S$  can be found such that one of the functions  $U_{1;\dots}, F_{1;\dots}$  vanishes if the elements of  $S$  are set to zero. In each subsector new subsectors are created, resulting in a tree-like structure after a certain number of iterations. The

book-keeping can be done with respective multi-indices. The iteration stops if the functions  $U_{1k_1 k_2 \dots}$ ,  $F_{1k_1 k_2 \dots}$  contain a constant term, i.e. if they are of the following schematic form

$$\begin{aligned} U_{1k_1 k_2 \dots} &= 1 + u(\mathbf{t}) \\ F_{1k_1 k_2 \dots} &= s_0 + \sum_X (s_X) f(\mathbf{t}) \end{aligned} \quad (13)$$

where  $u(\mathbf{t})$  and  $f(\mathbf{t})$  are polynomials in the variables  $t_j$  (without a constant term), and  $s_X$  are kinematic invariants, defined through (4). Thus, after a certain number of iterations, each integral  $G_1$  is split into a certain number, say  $R$ , of subsector integrals. For simplicity we replace the multi-index  $k_1 k_2 \dots$  stemming from the subsector decomposition by a single index which just counts the number of generated subsectors. Now, the produced subsector integrals are exactly of the same form as in Eq. (12), with the difference that the index  $k$  now runs from 1 to  $R$ , the total number of produced subsectors.

Evidently the singular behaviour of the integrand now can be trivially read off the exponents  $A_j, B_j$  for a given subsector integral ( $A_j, B_j$  are integers). The singular behaviour is manifestly non-overlapping now and thus it is straightforward to define subtractions. Before doing so a few comments are in order.

The described method cannot always lead to an optimal sector decomposition in the sense that the integral one starts with is split into the minimal number of subsector integrals, since obviously even finite integrals would be decomposed if a set  $S$  exists such that  $U$  or  $F$  vanish. The virtue of the algorithm lies in its easy programmability, as we introduced standardized representations suitable for iteration.

For massless 2-loop 4-point functions with 7 propagators and all external legs on-shell the number of generated subsectors is a few hundred. For 3-loop 3-point functions with two legs on-shell and 9 propagators it is a few thousand. Hence the bookkeeping of such numbers is only possible on a computer.

### Part III Extraction of the poles

The third part of the algorithm consists in a pole subtraction procedure for the subsector integrals  $G_{1k}$ . As the infrared sensitive variables now factorize in the subsector integrals, one can separate the part of the integrand which leads to  $\epsilon$ -poles.

Explicitly, the following procedure has to be worked through for each variable  $t_{j=1;\dots;N-1}$  and each subsector integrand:

The integrand of Eq. (12), characterized by the respective exponents  $A_j, B_j$  ( $j = 1;\dots;N-1$ ) of  $t_j$  and the functions of the form (13), can for each  $t_j$  be written as

$$I_j = \int_0^1 dt_j t_j^{(A_j - B_j)} I(t_j; \dots) \quad (14)$$

If  $A_j \geq 0$ , the integration does not lead to an  $\epsilon$ -pole. In this case no subtraction is needed and one can go to the next variable  $t_{j+1}$ . If  $A_j < 0$ , one expands  $I(t_j; \dots)$  into a Taylor series around  $t_j = 0$ . Using the definition  $I_j^{(p)}(0; \dots) = \partial^p I(t_j; \dots) / \partial t_j^p|_{t_j=0}$ , one obtains

$$I(t_j; \dots) = \sum_{p=0}^{A_j-1} I_j^{(p)}(0; \dots) \frac{t_j^p}{p!} + R(t_j; \dots) \quad (15)$$

Now the pole part can be extracted easily, and one obtains

$$I_j = \sum_{p=0}^{A_j-1} \frac{1}{A_j + p + 1} \frac{I_j^{(p)}(0; \epsilon)}{p!} + \int_0^{\epsilon} dt_j t_j^{A_j - B_j} R(t_j; \epsilon) \quad (16)$$

By construction the integral containing the remainder term  $R(t_j; \epsilon)$  does not get poles from the  $t_j$ -integration anymore. For example, in the generic case of a logarithmic divergence,  $A_j = 1$ ,  $p = 0$  and  $R(t_j; \epsilon) = I_j(0; \epsilon) - I_j^{(0)}(0; \epsilon)$ . Since, as long as  $j < N - 1$ , the expression (16) still contains an overall factor  $t_{j+1}^{A_{j+1} - B_{j+1}}$ , it is of the same form as (14) for  $j \rightarrow j + 1$  and the same steps as above can be applied to it.

After  $N - 1$  steps all singular integrations are done analytically and all poles are extracted. The resulting expression can be expanded in  $\epsilon$  now. This defines a Laurent series in  $\epsilon$  with coefficients  $C_{\text{lk},m}$  for each subsector integral  $G_{\text{lk}}$ . Since each loop can contribute at most one soft and collinear  $1/\epsilon^2$  term, the highest possible infrared pole of an  $L$  loop graph  $G$  is  $1/\epsilon^{2L}$ .

$$G_{\text{lk}} = \sum_{m=0}^{2L} \frac{C_{\text{lk},m}}{m!} \epsilon^m + O(\epsilon^{2L+1}) \quad (17)$$

Following the steps outlined above one has generated a regular integral representation of the coefficients  $C_{\text{lk},m}$ , consisting of  $(N - 1 - m)$ -dimensional finite integrals over parameters  $t$ .

Symmetries of the graph typically lead to equalities between primary sectors. It is thus useful to calculate the primary sectors  $G_1$

$$G_1 = \sum_{k=0}^{2L} G_{\text{lk}} \quad (18)$$

separately before summing over the  $l$  subsectors. In this way the symmetry relations provide a nontrivial check of the calculation.

## Part IV Calculation of the pole coefficients

Part four of the algorithm consists in the computation of the finite subsector integrals. The integrals contributing to the leading pole give ratios of polynomials in the Mandelstam variables. For the coefficient of the subleading pole one generally gets logarithmic terms. In principle, one can attempt to perform the  $(N - 1 - m)$ -dimensional integrations of all functions contributing to the coefficient of the  $1/\epsilon^m$  pole analytically. However, the sector decomposition produces many surface terms which will cancel only after summing up all subsector integrals, such that the analytical integrations become more and more involved for smaller values of  $m$ , especially if the graphs contain more than one scale, as for example in the case of 2-loop 4-point functions. For these functions only the coefficients of the leading and subleading poles could be obtained analytically by automatizing the integrations using Mathematica [33]. Pushing the analytical integrations further is possible only if some of the more complicated functions are manipulated "by hand" before feeding them into the subroutine, but this is tedious in view of the large number of functions to integrate. More powerful analytical integration routines, specialized to manipulations of polylogarithms and Nielsen functions [34] would be needed to allow for a complete analytical treatment.

On the other hand, the parametric integral representations are all very well suited for numerical integration, as long as the parametric function  $F$  has a definite sign. Then, it contains at most integrable, logarithmic divergences at the border of the integration domain. These generally present no problems for the numerical integrators which are on the market. If  $F$  is not of a definite sign, which means that one has to integrate over thresholds, the integrands contain poles inside the multi-dimensional integration domain. The presence of these poles typically considerably slows down, if

not hinders at all, the numerical evaluation of the integral. More advanced integration algorithms like e.g. the one proposed in [30] may solve this problem. We restrict ourselves to the case of definite sign here.

In most algebraic programs it is directly possible to create FORTRAN functions from a given expression. We fully automatized the translation of the expressions for the subsector integrals into the FORTRAN codes. For every primary sector we calculated the integral of the sum of the subsector integrands (18) with the Monte Carlo program BASES [31]. The integrations of all examples we calculated were totally stable. The limitation for the numerical integration comes thus only from CPU time, which increases with the number of loops and legs or, correspondingly, with the number of subsector functions. We will give more detailed information on program parameters in the examples below.

### 3 Applications

In this section we apply our method to calculate several nontrivial Feynman diagrams. To this end we implemented the algorithm outlined in section 2 into algebraic manipulation programs. To crosscheck the output we created two independent codes, one written in Maple [32], the other one in Mathematica [33]. First we show a comparison of the results obtained by our method with the results from the analytical calculation of the planar [13] and non-planar [14] massless double box. Then we give results for some 2-loop 4-point functions for which analytical results are not yet available in the literature, relevant for the calculation of certain higher order QCD corrections (see section 4). These are the massless planar and non-planar double box with one external leg on-shell, given in Figs. 1-3. As discussed above, our method so far only allows us to calculate numerical values of these graphs if all the Mandelstam variables have the same sign. In any case our result may serve as a nontrivial check of a future analytical computation of these graphs. Further we will give results for 3-loop 3-point graphs with two on-shell legs.

The numerical values given in subsection 3.1 contain a relative error of one percent. Note that for comparison purposes our conventions for the prefactors ( $\epsilon$ -functions) should be used since multiplying our results with conversion factors that are a power series in  $\epsilon$  may lead to a bad error propagation<sup>5</sup>. In subsections 3.2 and 3.3 we use a different prefactor than in subsection 3.1 because it leads to more compact expressions for the analytical result. This conversion may lead to errors in the numerical result which are slightly larger than one percent due to the error propagation mentioned above.

The numerical calculations were done on a DEC (ALPHA) workstation running with an EV6 processor. The CPU time needed ranges from about 5 hours for the planar two-loop graph up to about 3 days for the 3-loop graph with 9 propagators. The computer time needed is always dominated by the finite  $O(\epsilon^0)$  terms.

#### 3.1 Comparison with analytical results

In this subsection we compare our numerical approach with the analytical results for massless two-loop box diagrams calculated only recently [13, 14]. These results have also been crosschecked analytically meanwhile, and the perfect agreement with our results within the error of numerical integration confirms the reliability of our method.

##### The massless planar double box $B_7^P(s;t)$

The graph (see Fig. 1 with leg four on-shell) depends on the two kinematical invariants  $s = (p_1 + p_2)^2$  and  $t = (p_2 + p_3)^2$ . We show a comparison to the analytical result at two numerical points, the

---

<sup>5</sup>The reason is that multiplication with such a conversion factor mixes the different pole coefficients in our Laurent series, which can lead to a larger relative error in the converted result.



symmetric point  $s = t = -1$  and the asymmetric point  $(s;t) = (-1; -1/2)$ . As stated above, the physical situation  $st < 0$  is not suited for numerical evaluation in a straightforward manner because thresholds are present. In the following table we show the comparison between the analytical result of [13] and our numerical result for the relevant Laurent coefficients  $c_m^P(s;t)$  of the massless planar double box  $B_7^P(s;t)$ , defined through Eq. (3) and the subtraction algorithm :

$$B_7^P(s;t) = (-1)^7 (3+2)^{-X^4} \sum_{m=0} \frac{c_m^P(s;t)}{m} + O(\epsilon) \quad (19)$$

One can check that the agreement is always better than the demanded one percent.

$(s;t) = (-1; -1)$					
	$c_4^P$	$c_3^P$	$c_2^P$	$c_1^P$	$c_0^P$
analytical	-2.	6.	4.9167	-11.495	-13.801
numerical	-2.0000	6.0000	4.9188	-11.492	-13.811

$(s;t) = (-1; -1/2)$					
	$c_4^P$	$c_3^P$	$c_2^P$	$c_1^P$	$c_0^P$
analytical	-1.	3.8664	-0.38116	-9.2384	-2.9973
numerical	-1.0000	3.8664	-0.38059	-9.2377	-2.9990

Table 1: The massless planar double box. Comparison between analytical and numerical result for the points  $(s;t) = (-1; -1)$  and  $(-1; -1/2)$ .

### The massless non-planar double box $B_7^{NP}(s;t;u)$

Without using momentum conservation, the graph (see Fig. 2 with leg one on-shell) depends on the three kinematical invariants  $s = (p_1 + p_2)^2$ ,  $t = (p_2 + p_3)^2$  and  $u = (p_1 + p_3)^2$ . In the physical region one invariant is positive, leading always to an imaginary part. To avoid the corresponding threshold in the numerical integration we treated  $s;t;u$  as independent parameters. We compared to the analytical result of [14] by calculating numerically the coefficients  $c_m^{NP}(s;t;u)$  of the Laurent series of  $B_7^{NP}(s;t;u)$  (defined with the same conventions as in (19)) at the symmetric point  $s = t = u = -1$  and the asymmetric point  $(s;t;u) = (-1; -2; -3)$ , see Table 2.

### 3.2 Two-loop massless 4-point functions, one leg on-shell

Now we turn to the calculation of graphs where fully analytical results do not exist yet. The Mandelstam variables  $s, t, u$  are defined as above. If an external leg  $p_k$  is on-shell or on-shell but massive, we write  $p_k^2 = m_k^2$ . For the 4-point functions under consideration, exactly one leg is on-shell. Then momentum conservation implies  $s + t + u = m_k^2$ , but it has to be emphasized that this constraint has not been used to obtain the analytical results, in order to be able to compare them to numerical results for unphysical kinematics as well.

For sums of Feynman parameters we use short-hand notations like e.g.  $x_1 + x_j + x_k + x_l = x_{ijk1}$ .

$(s;t;u) = (1; 1; 1)$					
	$C_4^{N P}$	$C_3^{N P}$	$C_2^{N P}$	$C_1^{N P}$	$C_0^{N P}$
analytical	-1.75	3.	22.828	-113.63	395.26
numerical	-1.7500	2.9960	22.818	-113.75	393.08
$(s;t;u) = (1; 2; 3)$					
	$C_4^{N P}$	$C_3^{N P}$	$C_2^{N P}$	$C_1^{N P}$	$C_0^{N P}$
analytical	-0.4167	0.9310	5.8586	-42.760	162.81
numerical	-0.4167	0.9295	5.8748	-42.614	164.16

Table 2: The massless non-planar double box. Comparison between analytical and numerical result for the points  $(s;t;u) = (1; 1; 1)$  and  $(1; 2; 3)$ .

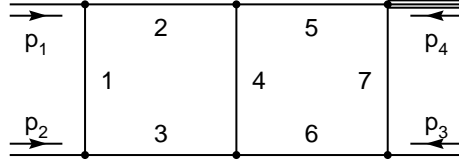


Figure 1: The planar double box with leg 4 on-shell.

The graph  $B_{7;lm ass}^P(s;t;u;m_4^2)$

With the labeling as in Fig. 1 one finds for the functions  $U, F$ :

$$\begin{aligned}
 U &= x_{123}x_{567} + x_4x_{123567} \\
 F &= (s)(x_2x_3x_{4567} + x_5x_6x_{1234} + x_2x_4x_6 + x_3x_4x_5) \\
 &\quad + (t)x_1x_4x_7 + (m_4^2)x_7(x_2x_4 + x_5x_{1234})
 \end{aligned} \tag{20}$$

The sector decomposition produces about 200 subsector integrals. For the leading and subleading pole we get the following analytical result:

$$B_{7;lm ass}^P = s^2(1 + \dots)(m_4^2)^{-2} \frac{1}{s^2t} - \frac{1}{4} - \frac{2}{3} \log(s=m_4^2) + \log(t=m_4^2) + O\left(\frac{1}{2}\right) \tag{21}$$

Numerically we find for the points  $(1=3; 1=3; 1=3; 1)$  and  $(1=2; 1=3; 1=6; 1)$ :

$$B_{7;lm ass}^P(1=3; 1=3; 1=3; 1) = s^2(1 + \dots) \frac{27.000}{4} - \frac{118.65}{3} - \frac{239.6}{2} - \frac{305.8}{1} - 164.1 \tag{22}$$

$$B_{7;lm ass}^P\left(\frac{1}{2}; \frac{1}{3}; \frac{1}{6}; 1\right) = s^2(1 + \dots) \frac{12.000}{4} - \frac{43.005}{3} - \frac{58.68}{2} - \frac{20.86}{1} + 97.63 \tag{23}$$

The graph  $B_{7;lm ass}^{NP}(s;t;u;m_1^2)$

With the labeling as in Fig. 2, the functions  $U, F$  are given by:

$$U = x_{123}x_{4567} + x_{46}x_{57}$$

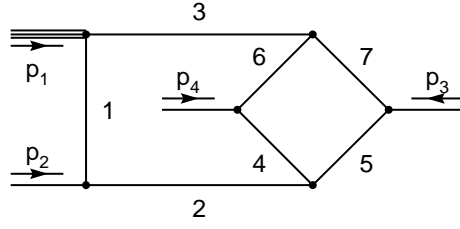


Figure 2: The non-planar double box with leg 1 on-shell.

$$F = (s)(x_2 x_3 x_{4567} + x_2 x_6 x_7 + x_3 x_4 x_5) + (t)x_1 x_4 x_7 + (u)x_1 x_5 x_6 + (m_1^2)x_1(x_6 x_7 + x_3 x_{4567}) \quad (24)$$

We note that this graph contains linear IR divergences, as it is the case if all legs are massless [14]. In a gauge theory, numerator functions would be present to prevent singularities of such strength. Since the subtractions are more complicated if linear divergences are present, the subsector integrands are more complicated as well. This leads to larger FORTRAN functions and thus slows down the numerical computation in comparison with the similar graph  $B_{7;lm\,ass;b}^{NP}$  below, which has poles stemming only from logarithmic divergences. It also requires a refined analytic integration routine. The sector decomposition produces about 250 subsector integrals. For the leading and subleading pole we obtain the following analytical result:

$$B_{7;lm\,ass;a}^{NP} = \frac{1}{4s^2tu} \frac{1}{4} (s+t+u-m_1^2 + \frac{tu}{m_1^2} + \frac{1}{2}(t+u)^2 + \frac{1}{3}h^2(3(s+t+u+m_1^2) + \log(s-m_1^2)[2(s+t+u-m_1^2) - 2\frac{tu}{m_1^2}(t+u)] + \log(t-m_1^2)[2(s+t+u-m_1^2) + 2\frac{tu}{m_1^2} + 3t-u] + \log(u-m_1^2)[2(s+t+u-m_1^2) + 2\frac{tu}{m_1^2} + 3u-t]) + O(\frac{1}{2}) \quad (25)$$

Numerically we find for the points  $(l=3; l=3; l=3; 1)$  and  $(l=2; l=3; l=6; 1)$ :

$$B_{7;lm\,ass;a}^{NP}(\frac{1}{3}; \frac{1}{3}; \frac{1}{3}; 1) = \frac{1}{4} (1 + \frac{8.997}{4} - \frac{101.7}{3} + \frac{592.7}{2} + \frac{3340}{1} + 18522) \quad (26)$$

$$B_{7;lm\,ass;a}^{NP}(\frac{1}{2}; \frac{1}{3}; \frac{1}{6}; 1) = \frac{1}{4} (1 + \frac{5.504}{4} - \frac{87.98}{3} + \frac{296.6}{2} + \frac{1753}{1} + 11741) \quad (27)$$

The graph  $B_{7;lm\,ass;b}^{NP}(s,t,u;m_3^2)$

With the labeling as in Fig. 3 one obtains for the functions  $U, F$ :

$$U = x_{123}x_{4567} + x_{46}x_{57} \\ F = (s)(x_2 x_3 x_{4567} + x_2 x_6 x_7 + x_3 x_4 x_5) + (t)x_1 x_4 x_7 + (u)x_1 x_5 x_6 + (m_3^2)(x_5 x_7 x_{12346} + x_2 x_4 x_7 + x_3 x_5 x_6) \quad (28)$$

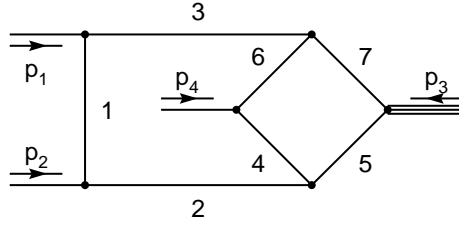


Figure 3: The non-planar double box with leg on-shell.

The sector decomposition produces about 230 subsector integrals. For the leading and subleading pole we obtain the following analytical result:

$$\begin{aligned}
 B_{7;1m\text{ ass},b}^{NP} = & \frac{1}{2} (1 + \epsilon) (m_3^2)^{-1/2} \frac{1}{2stu} \frac{1}{2^4} (t+u+4m_3^2) \\
 & + \frac{1}{3} \frac{h}{(t+u)} \log(s-m_3^2) \\
 & + (4m_3^2 - t+u) \log(t-m_3^2) \\
 & + (4m_3^2 + t-u) \log(u-m_3^2) + O\left(\frac{1}{2}\right)
 \end{aligned} \quad (29)$$

Numerically we find for the points  $(\epsilon=3; \epsilon=3; \epsilon=3; 1)$  and  $(\epsilon=2; \epsilon=3; \epsilon=6; 1)$ :

$$B_{7;1m\text{ ass},b}^{NP} \left( \frac{1}{3}; \frac{1}{3}; \frac{1}{3}; 1 \right) = \frac{1}{2} (1 + \epsilon) \left[ \frac{31.50}{4} - \frac{108.8}{3} - \frac{2.560}{2} + \frac{779.8}{1} \right] + 2395: \quad (30)$$

$$B_{7;1m\text{ ass},b}^{NP} \left( \frac{1}{2}; \frac{1}{3}; \frac{1}{6}; 1 \right) = \frac{1}{2} (1 + \epsilon) \left[ \frac{40.50}{4} - \frac{203.9}{3} - \frac{357.3}{2} + \frac{409.9}{1} \right] + 4608: \quad (31)$$

We recall that all the numbers given were calculated for unphysical kinematics (all particles ingoing) in order to have positive definite denominators. The numerical results for the 1-loop two-loop graphs as given above do not correspond to a physical situation. Nevertheless, they can easily be related to a physical process by the following reasoning. In the case of a  $1 \rightarrow 3$  process, e.g. a virtual particle with a squared momentum of  $m^2$  decaying into 3 massless particles,  $s, t, u$  and  $m^2$  are positive. By factoring out  $(-m^2)$  in the respective functions  $F$ , one gets again positive definite integrands. Especially, for a one-loop graph with  $N$  propagators, one finds

$$\begin{aligned}
 G^{2\text{-loop}}(s, t, u; m^2) &= (-m^2 - i\epsilon)^{N+4-2} G^{2\text{-loop}}(s=m^2; t=m^2; u=m^2; 1) \\
 &= \frac{1}{j_1^2 j_2^2 \dots j_{N+2}^2} \frac{(-1)^N e^{2i\pi}}{4+2} G^{2\text{-loop}}(s=m^2; t=m^2; u=m^2; 1)
 \end{aligned} \quad (32)$$

We introduced an infinitesimal imaginary part  $i\epsilon$  where necessary. This shows that our method allows to calculate 2-loop scalar integrals which appear for example in the calculation of the NNLO QCD corrections of  $e^+e^- \rightarrow 3$  jets, as explained in more detail in section 4.

### 3.3 Three-loop massless 3-point functions, one leg on-shell

Now we want to present results for 3-loop 3-point integrals with two legs on-shell. These contain only one scale which can be factored out of the integrand, such that one has to calculate a pure number which can be done numerically once and forever. We restrict ourselves to only two examples, the graphs shown in Figs. 4 and 5.

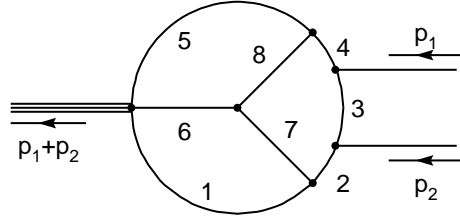


Figure 4: A 3-loop Mercedes-Star (MS) topology.

The graph  $MS_8(s)$

With the labeling as in Fig. 4, the functions  $U, F$  read:

$$\begin{aligned}
 U &= x_{23478}x_5x_{16} + x_{234}(x_6x_8 + x_1x_{68} + x_7x_{568}) + x_1x_7x_{68} + x_8(x_1x_6 + x_5x_7) \\
 F &= (s) x_1x_5(x_6x_{23478} + x_7x_8) + x_1x_4(x_6x_8 + x_7x_{568}) \\
 &\quad + x_2x_5(x_8x_{167} + x_6x_7) + x_2x_4(x_{17}x_{58} + x_6x_{1578})
 \end{aligned} \tag{33}$$

The sector decomposition produces about 1000 subsector integrals. We note that because of the symmetries of the graph only 5 of the 8 primary sectors as defined in Eq. (9) have to be calculated, i.e.  $MS_8^{sec_1} = MS_8^{sec_5}, MS_8^{sec_2} = MS_8^{sec_4}, MS_8^{sec_7} = MS_8^{sec_8}$ . On the other hand, the recalculation of these identical sectors are a good check of the algebraic/numerical computer routines. For the leading, subleading and subsubleading pole we find the following analytical result:

$$MS_8(s) = \frac{s^3(1+i)}{(s-i)^{2+3}} \frac{1}{36^6} + \frac{5(2)}{36^4} + O\left(\frac{1}{3}\right) \tag{34}$$

Numerically we find:

$$MS_8(s) = \frac{s^3(1+i)}{(s-i)^{2+3}} \frac{0.02778}{6} + \frac{0.0000}{5} + \frac{0.2288}{4} \frac{0.6692}{3} \frac{0.6152}{2} + \frac{2.005}{17.85} + 17.85 \tag{35}$$

The graph  $BBT_9(s)$

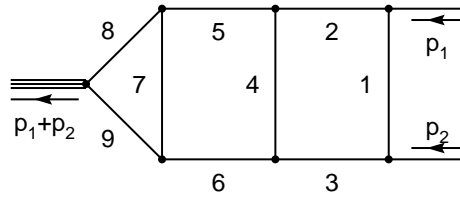


Figure 5: The 3-loop box-box-triangle (BBT) graph

With the labeling as in Fig. 5, the functions  $U, F$  are given by:

$$\begin{aligned}
 U &= x_{1234}x_7x_{89} + x_{789}(x_{123}x_{456} + x_4x_{56}) \\
 F &= (s) x_2x_3(x_{4567}x_{89} + x_7x_{456}) + (x_3x_5 + x_2x_6)x_4x_{789} + (x_3x_8 + x_2x_9)x_4x_7 \\
 &\quad + x_5x_6x_{1234}x_{789} + (x_6x_8 + x_5x_9)x_7x_{1234} + x_8x_9(x_{1234}x_{567} + x_{123}x_4)
 \end{aligned} \tag{36}$$

The sector decomposition produces about 2400 subsector integrals. For the leading and subleading pole we obtain the following analytical result:

$$BBT_9(s) = \frac{s^3(1+i)}{(s-i)^{3+3}} - \frac{1}{36} + O\left(\frac{1}{4}\right)$$

Numerically we find:

$$BBT_9(s) = \frac{s^3(1+i)}{(s-i)^{3+3}} - \frac{0.02778}{6} + \frac{0.0000}{5} - \frac{0.6852}{4} - \frac{2.072}{3} - \frac{6.613}{2} - \frac{25.07}{40.42} \quad (37)$$

## 4 Discussion

We want to discuss now the phenomenological applicability of our method to standard QCD processes. We will focus on reactions with massless particles in the loop. The first step of a multi-loop calculation is to express the corresponding amplitudes, preferably decomposed in colour and helicity space, in terms of basic tensor and scalar integrals. In the analytical approach one tries to express all tensor integrals by a certain set of scalar integrals, so-called master integrals. In a numerical approach it may be more convenient to calculate certain tensor integrals directly. In a Feynman parameter language this amounts to the calculation of integrals of the type (3), where one has in addition a polynomial  $A$  of Feynman parameters in the numerator. The generalization of our method to include these nontrivial numerators is straightforward. One way to proceed is to carry along the corresponding polynomial  $A$  through all the steps in addition to  $F$  and  $U$ , iterating the decomposition until  $A_{jk}$  contains also a constant term. This leads to an expression of type (12) with the integrand multiplied by  $A_{jk}$ . Part III and IV then work in exactly the same way as above. Since the presence of numerators in general improves the IR behaviour, the number of necessary subsector decompositions will be reduced, which typically shortens the computation time of the diagram under consideration as compared to the scalar case.

process	kinematics	scalar integrals	analytical	numerical
Drell-Yan, DIS to N <sup>3</sup> LO	2 ! 1	3-loop, 3-point, 1 mass	no	yes
	2 ! 2	2-loop, 4-point, 1 mass	no	yes ( )
	2 ! 3	1-loop, 5-point, 1 mass	yes	{
e <sup>+</sup> e <sup>-</sup> ! jjj;jj;j to NNLO	1 ! 3	2-loop, 4-point, 1 mass	no	yes
	1 ! 4	1-loop, 5-point, 1 mass	yes	{
PP;PP ! jj;j; to NNLO	2 ! 2	2-loop, 4-point	yes	yes ( )
	2 ! 3	1-loop, 5-point	yes <sup>z</sup>	{

Table 3: Knowledge on scalar integrals needed for various processes. In the column "analytical", results existing in the literature to O(<sup>0</sup>) are listed; those marked with z are known to all orders in . The column "numerical" shows where our method can improve the situation. The asterisk ( ) indicates that more powerful numerical integrators than the ones used in the present work would be needed to deal with thresholds.

In Table (3) we list some integrals entering the calculation of virtual corrections to phenomenologically relevant processes. We indicate for which ones analytical results exist in the literature and

where our numerical method improves the present situation. For the calculation of the NNLO QCD corrections of  $e^+e^- \rightarrow jjj; jj; j$  two-loop box graphs with one massive external leg are needed. As has been demonstrated above these diagrams can be calculated numerically with our method. This is also true for 3-loop 3-point functions needed for a N<sup>3</sup>LO calculation of deep inelastic scattering (DIS) and the Drell-Yan process<sup>6</sup>. Although our algorithm produces integrable functions which in principle always allow for a numerical evaluation, the presence of thresholds inside the integration region worsens the convergence properties of an integration routine. These cases are marked with an asterisk (\*) in Table 1. It means that more efficient numerical integrators than the ones we used would be needed.

After having calculated the purely virtual corrections of say a 2 + N process involving L-loop integrals, the latter have to be combined with the 2 + N + 1 corrections which include (L - 1)-loop integrals and where one has to integrate over the extra (unobserved) particle. This integration produces soft/collinear poles which require the knowledge of the respective (L - 1)-loop integrals to O( $\epsilon^2$ ), at least in the corresponding IR regions, since they have to be combined with these singular phase space integrals. However, most of the existing analytical results are known only to O( $\epsilon^0$ ). In the context of our method, expansion of the results for the virtual integrals up to higher orders in  $\epsilon$  constitutes no principle problem, only the size of the FORTRAN routines will increase.

In conclusion, we have presented a simple, constructive subtraction algorithm to deal with IR divergent multi-loop integrals. Although the iterated sector decomposition produces in general a relatively large number of subsector integrals, we demonstrated that by means of automatization our method allows for the numerical computation of highly nontrivial Feynman diagrams of two- and three-loop type. We pointed out that with our numerical approach, certain higher order QCD calculations can be tackled without waiting for further developments of analytical methods.

---

<sup>6</sup>We note that this refers only to the calculation of the partonic cross section; for a complete analysis, the splitting functions also have to be known to this order.

## Acknowledgments

We thank Bas Tausk for a fruitful exchange of ideas. His analytical calculations served not only as a benchmark for our algorithm, but also triggered the rigorous development from the initial idea to the final code. Further we would like to thank V. A. Smirnov for useful discussions. We also are grateful to J. Ph. Guillet for helpful discussions and comments on the manuscript. G. H. would like to thank the LAPTH for its hospitality during various visits.

This work was supported by the EU Fourth Training Programme "Training and Mobility of Researchers", Network "Quantum Chromodynamics and the Deep Structure of Elementary Particles", contract FMRX-CT98-0194 (DG 12-MHT).

## References

- [1] S. G. Gorishnii, A. L. Kataev and S. A. Larin, Phys. Lett. B 259, 144 (1991);  
M. A. Samuel and L. R. Surguladze Phys. Rev. Lett. 66, 560 (1991).
- [2] T. van Ritbergen, J. A. Vermaseren and S. A. Larin, Phys. Lett. B 400, 379 (1997).
- [3] F. V. Tkachov, Phys. Lett. B 100, 65 (1981);  
K. G. Chetyrkin and F. V. Tkachov, Nucl. Phys. B 192, 159 (1981).
- [4] A. G. Grozin, hep-ph/0002266.
- [5] R. J. Gonsalves, Phys. Rev. D 28, 1542 (1983).
- [6] G. Kramer and B. Lampe, Z. Phys. C 34, 497 (1987); E: C 34, 504 (1989).
- [7] T. Matsuura and W. L. van Neerven, Z. Phys. C 38, 623 (1988);  
T. Matsuura, S. C. van der Marck and W. L. van Neerven, Nucl. Phys. B 319, 570 (1989).
- [8] N. I. Usyukina and A. I. Davydychev, Phys. Lett. B 348, 503 (1995).
- [9] A. I. Davydychev and P. Osland, Phys. Rev. D 59, 014006 (1999).
- [10] E. B. Zijlstra and W. L. van Neerven, Nucl. Phys. B 383, 525 (1992);  
ibid Phys. Lett. B 297, 377 (1992);  
Nucl. Phys. B 417, 61 (1994); E: Nucl. Phys. B 426, 245 (1994).
- [11] R. Hamberg, W. L. van Neerven and T. Matsuura, Nucl. Phys. B 359, 343 (1991);  
W. L. van Neerven and E. B. Zijlstra, Nucl. Phys. B 382, 11 (1992).
- [12] Z. Bern, L. Dixon and D. A. Kosower, JHEP 0001, 027 (2000) [hep-ph/0001001].
- [13] V. A. Smirnov, Phys. Lett. B 460, 397 (1999) [hep-ph/9905323].
- [14] J. B. Tausk, Phys. Lett. B 469, 225 (1999) [hep-ph/9909506].
- [15] C. Anastasiou, E. W. N. Glover and C. Oleari, Nucl. Phys. B 565, 445 (2000)  
and hep-ph/9912251.
- [16] V. A. Smirnov and O. L. Veretin, Nucl. Phys. B 566, 469 (2000) [hep-ph/9907385].
- [17] T. Gehrmann and E. Remiddi, hep-ph/9912329.



- [18] C . Anastasiou, T . Gehrmann, C . Oleari, E . Remiddi and J . B . Tausk, hep-ph/0003261 .
- [19] D . Kreimer, Phys. Lett. B 347, 107 (1995);  
R . Kreckel, D . Kreimer and K . Schilcher, Eur. Phys. J. C 6 (1999) 693 [hep-ph/9804333].
- [20] D . E . Soper, hep-ph/9910292 and Phys. Rev. Lett. 81 2638 (1998).
- [21] T . Kinoshita, A . Ukwai, Phys. Rev. D 15, 1596 (1977).
- [22] J . C . Collins, D . E . Soper, G . Sterman, in Perturbative Quantum Chromodynamics, ed. A . H . Mueller, World Scientific, Singapore 1989.
- [23] V . A . Smirnov, Renormalization and asymptotic expansion, Birkhauser Verlag Basel 1991.
- [24] N . Nakanishi, Graph Theory and Feynman Integrals, Gordon and Breach, New York 1971.
- [25] O . I . Zavialov, Renormalized Quantum Field Theory, Kluwer 1990. Translation of a Russian book published in 1979.
- [26] C . Itzykson, J . B . Zuber, Quantum Field Theory, World Scientific 1993.
- [27] L . Landau, Nucl. Phys. 13, 181 (1959).
- [28] G . Sterman, Phys. Rev. D 17 2773 (1978).
- [29] K . Hepp, Commun. Math. Phys. 2, 301 (1966).
- [30] S . Jadach, physics/9910004, submitted to Comp. Phys. Commun.
- [31] S . Kawabata, Comp. Phys. Commun. 88 (1995) 309.
- [32] Maple by Waterloo Maple Corp.; see Maple V Language Reference Manual, Springer Verlag 1991.
- [33] S . Wolfram, Mathematica Version 3.0 .
- [34] L . Lewin, Polylogarithms and associated functions, North Holland 1981;  
K . S . Kolbig, J . A . Mignaco, E . Remiddi, BIT 10, 38 (1970).